INTERNATIONAL JOURNAL OF PHARMACY WITH MEDICAL SCIENCES
Peer Reviewed, Referred & Indexed Journal
E-ISSN:3068-2738
Vol.6, No. 2(2026)
www.ijpams.com

CARALLUMA-MEDIATED GREEN SYNTHESIS OF AG–FE "BIMETALLIC NANOPARTICLES" FOR OPTICAL, STRUCTURAL APPLICATIONS

Konathala Sirisha Rani [1], K Suresh Babu[2*], Boyapati Veeranjaneyulu [3]
[1]Research Scholar, BEST Innovation University, Gownivaripalli, Gorantla, Andhra Pradesh 515231, India.
[1]Asst Professor, St Pious X Degree and PG College for Women, Nacharam, Secunderabad
[2] Department of Chemistry, Marri Laxman Reddy Institute of Technology and Management, Hyderabad, India.
[3]Department of Chemistry, Kakaraparti Bhavanarayana College, Vijayawada, Andhra Pradesh-520001.India.
Corresponding author:
Dr K Suresh Babu
E Mail: babuiict@gmail.com, sureshbabuiict1@gmail.com

Abstract
The use of plant extract in the green production of "bimetallic nanoparticles" is gaining traction in the scientific community. 'nanoparticles' of Ag-Fe were created by employing the extract of the Caralluma lasaintha plant as a bio-reducing and stabilising agent. In order to examine the nanoparticles' structural integrity, we compared the as-prepared (IAF-P) and thermally treated (IAF-T) 'Ag–Fe' nanoparticles. 'nanoparticles' were stabilised and formed in part by plant biomolecules, as shown by FTIR data that verified the presence of phytochemical functional groups such as hydroxyl, carbonyl, and 'C-O' groups. The XRD results showed that both the untreated and thermally treated samples included crystalline nanoparticles, with an average crystallite size of 22 nm and 28 nm, respectively. The wide absorption band in the 300-350 nm range of the UV-visible spectra was observed in the optical response 'Ag–Fe' nanoparticle system, which is worth mentioning.SEM micrographs showed porous and agglomerated structures of 'nanoparticles' in the raw sample, and the relatively compact granular and rod-like structures of the thermally treated sample because of the enhanced particle growth. The analysis of Dielectric shows a reduction in frequency with regards to dielectric loss and dielectric constant which was similar to the behaviour of Maxwell-Wagner interfacial polarization. Thermal treatment led to better dielectric stability and moderately increased AC conductivity of the thermally treated 'nanoparticles' through increased crystallinity and fewer organic residues. Therefore, a green synthesis to catalysis, functional nanomaterials, and nanoelectronics synthesis is the green synthesis of 'Ag–Fe' "bimetallic nanoparticles" using Caralluma.

Keywords: Green synthesis, *Caralluma* extract, 'Ag–Fe' nanoparticles, Surface plasmon resonance, Dielectric properties, Bimetallic nanomaterials.

1. Introduction

The idea of nanotechnology has greatly changed the nature of modern materials science as nanoscale materials with distinctive optical, electrical and catalytic characteristics can be produced using nanotechnology. 'nanoparticles' are useful in many fields, including electronics, biomedical engineering, environmental remediation, and catalysis, thanks to their elevated surface-to-volume ratio and quantum confinement effects, which enhance their physicochemical properties[1], [2].

Silver 'nanoparticles' (AgNPs) are one of the nanomaterials that have gained much interest because of their optical properties, especially localised surface plasmon resonance (LSPR), which occurs when electrons of the conduction band collectively vibrate in response to electromagnetic radiation [3], [4].

The applications of these optical characteristics have been in sensors, biomedical devices, antimicrobial coatings, and photonic materials utilizing silver nanoparticles.

The addition of a second metal to silver 'nanoparticles' tends to increase structural stability and physicochemical characteristics. In bimetallic nanoparticles, metals have synergistic interactions with each other leading to superior catalytic, electrical conductivity and magnetic properties [4], [5]. 'Ag–Fe' 'nanoparticles' are among many other bimetallic systems which have received interest due to the multifunctionality of the system which can be applied to catalytic, environmental and electronic applications owing to the combination of plasmonic and magnetic iron. Traditional methods for preparing 'nanoparticles' frequently involve the use of harmful chemicals such as sodium borohydride and hydrazine, which can result in environmental pollution and health hazards [6].

Consequently, there is significant interest in environmentally friendly synthesis methods.

Plant extracts Green synthesis has also become a viable alternative to the conventional chemical synthesis techniques. Plant extracts have rich phytochemicals like flavonoids, phenolics, alkaloids, and terpenoids that may be used as natural reducing agents in the nanoparticle synthesis and also biomolecular capping of the 'nanoparticles' [7].

The species of *Caralluma lasaintha* have become of interest among other medicinal plants because of their abundant phytochemical makeup. Some physiologically active chemicals, including as pregnane glycosides, flavonoids, and phenolic compounds, are abundant in the plant and possess a high reducing capacity [8], [9]. These phytochemicals have the capacity to stabilise the resulting nanostructures by reducing metal ions to nanoparticles. Other than synthesis, electrical and dielectric behavior of nanomaterials is also worth understanding to be applied in electronic devices and energy storage systems. Dielectric measurements are useful in the study of polarization processes, charge transport processes and relaxation of nanostructured material[10].

Numerous researches have examined the creation of metallic and "bimetallic nanoparticles" using plant-mediated processes, utilising a variety of biological extracts. For instance, Karthik et al. [11] reported the biosynthesis of silver 'nanoparticles' using Azadirachta indica leaf extract. It was demonstrated that phytochemicals, including flavonoids and terpenoids, served as stabilising and reducing agents, resulting in 'nanoparticles' with sizes ranging from 10 to 50 nm and exhibiting strong plasmonic absorption in the visible wavelength. Similarly, the green synthesis of metallic 'nanoparticles' was explored through various plant extracts, highlighting its environmental safety and improved biological compatibility compared to alternative chemical synthesis methods[12]. Further, another study summarized the review of plant-mediated nanoparticle preparation and highlighted how essential polyphenols, alkaloids, and phenolic compounds were in regulating nanoparticle nucleation, growth, and stabilization[13]. Another study more recently described the synthesis of plant-derived "bimetallic nanoparticles" and found that by combining two metals many synergies could be created in catalytic activity, electrical conductivity, and structural stability by metal to metal interaction[14], [15]. Nevertheless, the majority of these studies were mainly on monometallic 'nanoparticles' or general synthesis, and none of the systematic research was done to study plant-mediated 'Ag–Fe' bimetallic nanoparticles, especially with *Caralluma* species as the reducing agent. Moreover, in academia the impact of thermal treatment on morphological change, thermal treatment on the structural development and dielectric response of 'Ag–Fe' 'nanoparticles' synthesis remains to be explored. The objective of this study is to integrate 'Ag–Fe' "bimetallic nanoparticles" with Caralluma plant extracts and to assess the impact of thermal treatment on the morphology, structure, optical properties, and dielectric functions of the nanoparticles. This research aims to enhance understanding of the property-structure relationship of multifunctional 'nanoparticles' derived from Caralluma plant extract.

As a consequence, this study focuses on the green synthesis of 'Ag–Fe' "bimetallic nanoparticles" using Caralluma plant extract, along with an investigation of their structural, optical, and dielectric properties.

2. Experimental Section

2.1 Materials

The precursor salts, such as silver nitrate (AgNO3) and ferric nitrate, along with additional chemicals like sodium hydroxide (NaOH) and distilled water, are obtained from Sigma Aldrich, Chennai. All chemicals were obtained in analytical reagent (AR) grade to ensure purity.The C*aralluma lasaintha* stem was given by the herbium keeper in the Tirumala Forest. It was observed that the samples were healthy and did not contain insect growth in India.

Figure1 Caralluma lasaintha plant

2.2 Method of extraction of plant extract

The fresh stems of *Caralluma* plant were gathered in the area and processed into plant extract. Proper cleansing of the plant material was done twice with distilled water and dried in a shady place that was followed by grinding of the plant material in a mortar and pestle into small pieces. It is a plant material in powder form. A soxhlet extractor was used to extract a quantitative amount of powder that had been sieved and stored. Repeated solvent extraction was carried out by use of solvents of increasing polarities (hexane).

2.3 Ag Fe 'nanoparticles' Green Synthesis

To prepare green nanoparticles, approximately 1mg of silver nitrate and 1mg of ferric nitrate were each dissolved in 25ml of distilled water in a separate 50ml glass beaker. The two solutions were subsequently combined in a beaker containing 1000 ml of water and stirred continuously using a magnetic stirrer for 10 minutes at a speed of 1000 rpm. Approximately 50ml of plant extract was placed in a burette and gradually added to the precursor solution until a change in colour was observed. When silver salt is combined with plant extracts, the colour of the solution changes with time. After that about 17ml of NaOH solution was added slowly using burette for the reduction of 'nanoparticles' which are formed. Subsequently, the mixture was put in a magnetic stirrer and agitated for two hours at 1000 rpm. It was then let to sit for a few minutes and stirred again for another two hours. After that, the reaction mixture was heated in a mantle at 60 °C. The transition from colourless to brown was the full reduction of AgNO3 to Ag+ ions [16]. The mixture was let cool down to room temperature. Three times in a row, the NPs were cleaned with deionised water. The finished NPs were spun in a centrifuge and then dried in a hot air oven for two hours at 80oC. This is called IAF-P.The sample was powdered well and heated to 300°C and this was mentioned as IAF-T. The final samples were utilized for the characterisation analysis.

3. Characterisation analysis

3.1 FTIR Analysis

Fourier Transform Infrared Spectroscopy (FTIR) was used to find the phytochemical capping agents and surface functional groups of the Ag–Fe "bimetallic nanoparticles" that were made.The spectra data were taken with the help of FTIR spectrometer (PerkinElmer Spectrum Two, PerkinElmer Inc., USA) with the attenuated total reflectance (ATR) accessory[17], [18]. About 2 - 3 mg of dry nanoparticle powder (IAF-P and IAF-T) were immediately applied on the ATR crystal and carefully pushed to guarantee a secure connection. The spectra were taken in the 4000-400 cm-1 wavenumber region with a resolution of 4 cm-1 and 32 cumulative scans to improve the signal-to-noise ratio. Before each measurement, the background was adjusted. The spectra helped us find several functional groups that were derivatives of the Caralluma phytochemicals and helped the 'Ag–Fe' 'nanoparticles' stay stable and less reactive.

3.2 UV–Visible Analysis

Researcher used UV-Visible spectroscopy to look at the optical absorption properties and the production of 'Ag–Fe' bimetallic nanoparticles. Researcher used a Shimadzu UV-2600spectrophotometer (Shimadzu Corporation, Japan) [19], [20] to get the absorption spectra. To quantify it, a homogeneous suspension was created by putting around 1 mg of nanoparticle powder in 10 mL of deionised water and shaking it with ultrasonic waves for 10 minutes. The dispersion was transferred to a quartz cuvette with a 1 cm path length, and the spectra were collected in the 200-800 nm wavelength range at a scan rate of 600 nm min-1. Deionised water was used to make the reference blank. The production of 'nanoparticles' and their optical characteristics were evaluated utilising the distinctive absorption bands.

3.3 XRD Analysis

The phase composition and crystalline structure of the produced 'Ag–Fe' "bimetallic nanoparticles" were determined using X-ray diffraction (XRD) analysis. The X-ray diffractometer data was obtained using Cu-α radiation (λ= 1.5406Å), operating at 40kV and 30mA, utilising a Bruker D8 Advance from Germany [21].To analyse the samples, a smooth surface of the nanoparticle sample (IAF-P and IAF-T) on a glass sample holder was levelled with a fine powder of about 100 mg. The diffraction patterns were recorded over a 2θ range of 10° to 80° with a spacing step of 0.02° and a scan rate of 2° per minute. The diffraction peaks obtained were indexed to determine crystalline phases and measure such structural properties as crystallite size and lattice parameters.

The Debye-Scherrer equation was utilised to estimate the average size of the crystallites in the synthesised nanoparticles.

$$D = {K\lambda}/{\beta\cos\theta} \qquad (1)$$

D represents the crystallite size, K refers to the form factor (0.9), λ indicates the X-ray wavelength (0.15406 nm), and λ also refers to the full width at half maximum (FWHM) of the diffraction peak, while θ signifies the Bragg diffraction angle.

3.5 SEM Analysis

Scanning electron microscopy (SEM) was utilised to investigate the surface morphology and particle distribution of the synthesised nanoparticles. The SEM analysis was conducted utilising a field emission scanning electron microscope (FESEM, JEOL JSM-7600F, JEOL Ltd., Japan)[22].A tiny quantity of the dried powdered nanoparticle (about 5 mg) was deposited on a carbon-coated aluminium stub using double-sided conductive carbon tape to create the sample. The sample was then coated with a 60-second gold sputter to enhance its electrical conductivity. The imaging was conducted under high vacuum conditions with an accelerating voltage ranging from 10 to 15 kV. The micrographs obtained were

utilised to identify the morphology of the particles, their aggregating behaviour, and the approximate size distribution.

3.6 Dielectric Properties

The dielectric behaviour of the synthesised Ag–Fe 'nanoparticles' was assessed using an LCR impedance analyser (Keysight E4980A Precision LCR Meter, Keysight Technologies, USA). For dielectric measurements, approximately 200 mg of the nanoparticle powder (IAF-P and IAF-T) was compressed into a circular pellet with a diameter of 10 mm and a thickness of about 1 mm using a hydraulic pellet press at a pressure of 5 tonnes. Silver paste was applied to the surfaces of the pellets to form conductive electrodes and was dried at 60°C for 30 minutes [23]. The dielectric constant (C), dielectric loss (tan δ), and AC conductivity were assessed at room temperature across a frequency range of 100 Hz to 1 MHz. The results were collected and used to determine the dielectric response and polarisation processes of the produced 'nanoparticles' through a parallel plate capacitor configuration.

3.7 In silico docking study

The docking study performed using Biovia Discovery Studio with C-Docker provides crucial insights into the potential binding interactions between various plant-derived compounds and protein targets. Important markers of the stability and strength of these interactions are the C-Docker energy and C-Docker Interaction energy values.The docking scores were calculated across multiple targets, and these results help identify the most promising plant derivatives for further exploration. Below is a comprehensive analysis of the results. C-Docker Energy: This energy value represents the total energy of the ligand-receptor complex in the docking pose. More negative values indicate greater stability of the binding, suggesting a stronger and more favourable interaction. C-Docker Interaction Energy: This specific energy value reflects the strength of non-bonded interactions (like van der Waals, electrostatic interactions, and hydrogen bonding) between the ligand (the plant derivative) and the target protein. A more negative value signifies stronger interaction energy, indicating a more stable and potent binding.

3.8 DPPH Radical Scavenging

The plant extract's antioxidant activity was evaluated using the DPPH radical scavenging test. 3.94 mg of DPPH were dissolved in 100 mL of methanol to create a 0.1 mM solution, which was then kept out of direct sunlight in an amber-colored bottle. Ten milligrams of the dried extract were dissolved in ten millilitres of methanol to create a stock solution of the plant extract with a concentration of one milligram per millilitre. This stock solution was serially diluted with methanol to create concentrations of 20, 40, and 60 µg/mL. In test tubes with labels, 1 mL of each plant extract concentration and 1 mL of the 0.1 mM DPPH solution were combined for the assay. One millilitre of DPPH solution and one millilitre of methanol were combined to create a control. After a gentle vortex, each mixture was allowed to sit at room temperature for half an hour in the dark. Following incubation, a UV-Visible spectrophotometer was used to measure the absorbance of each sample, standard, and control at 517 nm. It was determined what proportion of DPPH radicals were inhibited. The average absorbance values were noted after the experiment was carried out three times.

3.9 Anti-fungal activity

Aspergillus fumigatus, Candida tropicalis, and Trichophyton rubrum were the three fungal strains against which the samples' antifungal activity was assessed using the agar well diffusion method. A fungal culture that was 24 to 48 hours old was suspended in sterile saline and its turbidity was adjusted to the 0.5 McFarland standard in order to create a fungal inoculum. After preparing nutrient agar plates, a sterile cotton swab was used to evenly distribute the fungal suspension across the agar surface. A cork borer was then used to make wells, into which 50–100 µL of each test sample was added. For comparison, both positive and negative controls were used. For 24–48 hours, the plates were incubated at 28–30°C for moulds and 35–37°C for yeast. The antifungal activity was assessed by measuring the zones of inhibition in millimetres following incubation; bigger zones denoted more inhibition.

3.10 *In-vitro* Anti diabetic assessment

First, a 1% soluble starch solution and a 1% α-amylase enzyme solution in phosphate buffer (pH 6.8) were prepared for the α-amylase inhibition experiment for Caralluma extract. "Caralluma extract" was dissolved in the appropriate solvent at concentrations of 50, 100, and 200 µg/mL. In several clean test tubes, I mixed 500 µL of the extract and 500 µL of the enzyme solution. After that, I incubated the mixture for ten minutes at 37°C. I then added 500 µL of the starch solution and let it sit for an additional 10 minutes. After adding 1 mL of DNSA reagent to stop the reaction, the tubes were submerged in boiling water for five minutes to develop the colour. Following cooling, the solutions were diluted with distilled water, and a UV-Visible spectrophotometer was used to detect absorbance at 540 nm. The formula based on the absorbance of the test and control samples was used to determine the % inhibition. The assay revealed that Sample 13 inhibited α-amylase in a dose-dependent manner, with larger inhibitory effects at higher doses.

4. Result and Discussion

4.1 FTIR analysis

Figures 2(a) and 2(b) of the IAF-P (plant extracted nanoparticles) and "IAF-T" (thermally treated nanoparticles) samples, respectively, display the "Fourier Transform Infrared (FTIR)" of the synthesised Ag–Fe "bimetallic nanoparticles" extracted by Caralluma. The spectra are helpful in identifying the phytochemical functional groups involved in the reduction, stabilisation, and surface modification of the nanoparticles. A wide, strong absorption band with a peak at 3364 cm 3364 cm-1 is present in the IAF-P spectrum. The O-H stretching vibration of the hydroxyl groups of the alcohols and phenols in the "Caralluma extract" is linked to this band. In addition to stabilising the resultant 'nanoparticles' by creating "hydrogen bonds, it has been established that these hydroxyl groups play a crucial role in the reduction of Ag+ and Fe3+ ions into metallic nanoparticles."This broad OH stretching band is also observed in the "IAF-T" sample at 3369 cm^{-1} with weaker band, which suggests that organic residues in the sample were partially removed or transformed as a result of "thermal treatment". The "absorption band at 2362 cm^{-1}in IAF-P and 2361 cm^{-1}in "IAF-T" is associated with either ambient CO2 or C-H stretching vibrations."The fact that the change between the two samples is minimal implies that whatever thermal treatment method is applied, there is no significant change that induces this vibration. "The C=O stretching vibrations of carbonyl functional groups, which may be attributed to aldehydes, ketones, or ester groups on plant biomolecules, are the cause of the IAF-P signature of 1737 cm-1 is a approximatepeak." Nevertheless, the "IAF-T" spectrum exhibits a lesser prominence of this peak, suggesting that some organic functional groups are destroyed during the heating process. "Furthermore, H-O-H bending or aromatic C=C vibrations are attributed to the band at 1581 cm^{-1}in IAF-P and 1584 cm-1 in IAF-T."These vibrations may be the result of polyphenolic chemicals or the presence of adsorbed water molecules that are associated with the nanoparticle's surface. The minor movement and the change in intensity of the two samples indicate that there was a structural change in the organic capping agents on heating. "Both spectra have a strong peak of absorption of 1363 cm^{-1} that is attributed to C-H bending vibrations, which are commonly linked to aliphatic groups found in biomolecules of plants. The band at 1018 cm^{-1} in the lower wavenumber is the one that is ascribed to 'C-O' stretching vibrations, which are typically attributed to alcohol, ethers or glycosidic bonds." This maximum is typical of polysaccharides and other compounds with carbohydrate basis in the plant extract that serve as natural stabilizing and capping agents in the creation of nanoparticles. "The presence of carbohydrate-derived compounds that stabilise 'nanoparticles' is suggested by the absorption at 877 cm-1, which is also ascribed to β-glycosidic linkages."The thermal treatment causes partial loss or alteration of phytochemical capping agents and thus, results in a higher degree of crystallinity in 'nanoparticles' without the loss of certain surface functional groups that maintain the stabilization process. These results agree with earlier reports about the synthesis of metal 'nanoparticles' through

plants, in which phenolic compounds, proteins and carbohydrates served as reducing and stabilization agents[20]. The "FTIR characteristics of green synthesised Ag and Fe 'nanoparticles' in the plant extracts have been reported to be similar.These 'nanoparticles' show distinctive OH stretching bands at 3300-3400 cm^{-1}, carbonyl bands at around 1700 cm^{-1}, and CO bands at about 1000 cm^{-1}, indicating the involvement of plant biomolecules in the nanoparticles' production and stabilisation." The findings therefore show that the attenuation of metal ions and the stability of the resulting 'Ag–Fe' "bimetallic nanoparticles" depend on Caralluma extract.

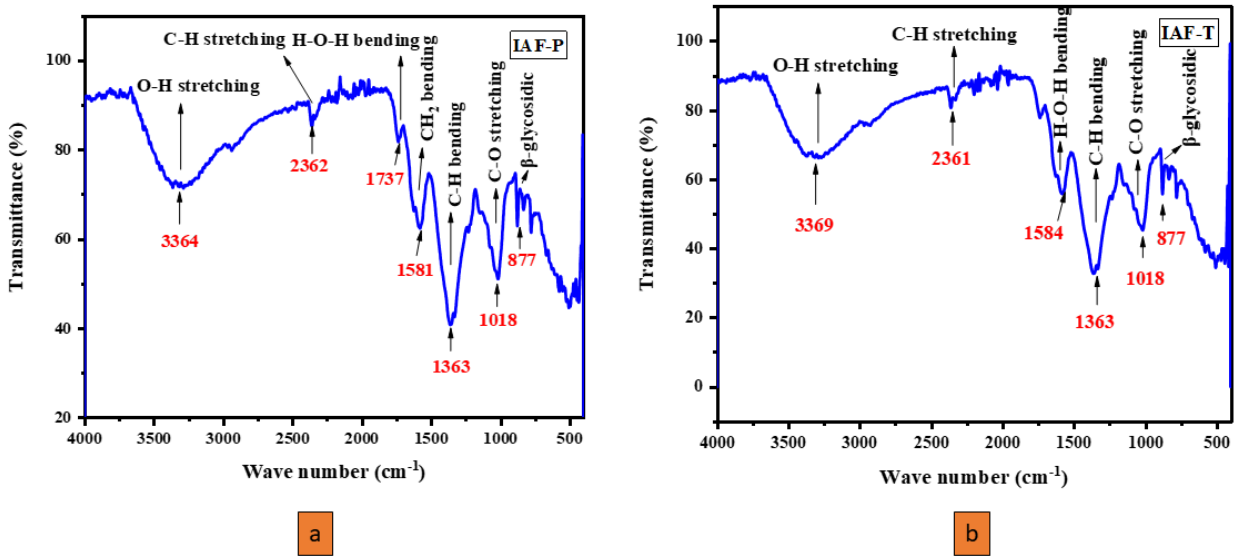

Figure 1 "FTIR peak analysis" of a) Pre-extracted b) thermal treated green 'Ag–Fe' bimetallic nanoparticle

4.2 X-Ray diffraction analysis

X-ray diffraction was used to determine the crystalline structure and phase composition of the Ag–Fe "bimetallic nanoparticles" generated in the presence of Caralluma. Figures 3a and 3b display the diffraction patterns of the IAF-P and "IAF-T" samples, respectively. The diffraction peaks in both patterns are distinct, so guaranteeing that the crystalline phases of the nanoparticle are achieved.

In the case of "IAF-P the peaks of the diffractogram were at 2θ, 28.03°, 32.39°, 38.41°, 44.45°, 46.31°, 64.37° and 77.66°. The face-centered cubic (fcc) silver (111) plane, which has a strong peak at 38.41o, is consistent with the conventional diffraction pattern of metallic silver (JCPDS card No. 04-0783)."" The crystalline structure of silver 'nanoparticles' is indicated by additional reflections of the (200) and (311) planes of fcc Ag at 44.45o and 77.66o, respectively. The iron oxide phases may be responsible for the peaks at 32.39o and 46.31o, which are in line with the iron oxide/ferrite diffraction patterns (JCPDS No. 19-0629). The identification of these diffraction peaks also indicates the successful synthesis of 'Ag–Fe' "bimetallic nanoparticles" using the plant-mediated synthesis pathway."

"The diffraction peaks of "IAF-T" sample are similar to those of the IAF-P sample at 2θ = 28.03°, 32.39°, 38.50°, 44.40°, 46.57°, 64.68°, and 77.76° respectively. The thermally treated sample is, however, more crystalline with sharper and stronger peaks in the thermally treated sample."" The prevailing reflection at 38.50° of the (111) plane of Ag also gives the typical pattern of metallic silver (JCPDS No. 04-0783)." The minor change in the positions of peaks and the increase in the intensity indicate better lattice arrangement and some elimination of organic remains of biomolecules in plants as a result of thermal treatment.

"Using equation 2, researchers were able to determine that the average size of the crystallites reflecting 111 nm was approximately 22 nm and 28 nm for IAF-T, respectively." This indicated that there was moderate particle growth following thermal treatment."Secondly, the crystallinity index (CI) also rose, as it was approximately from 72% to 84% after thermal treatment, indicating that the thermally treated specimen had a better structural ordering. Table 1 provides a comparison of the crystallite size (CS) and a crystal domain growth index (CI) values obtained on plant-mediated "bimetallic nanoparticles" synthesized using different plant extracts." In the vast majority of works on green synthesis, phytochemical capping agents on the surface of the 'nanoparticles' result in smaller crystallite sizes and comparatively lower crystallinity indices, though this may be varied according to the phytochemical used. As the thermal treatment is carried out, the organic residues are usually removed, with better atomic ordering, leading to increased crystallite size and increased crystallinity. The results confirmed the successful preparation of crystalline "Ag –Febimetallic nanoparticles" with the thermal treatment enhanced crystallinity and crystal domain growth.

Table 1 Comparison of crystallite size (CS) and crystallinity index (CI) of plant-mediated bimetallic nanoparticles

S.No	Plant Source	Nanoparticle System	CS – Raw (nm)	CS – Heat Treated (nm)	CI – Raw (%)	CI – Heat Treated (%)	Reference
1	*Caralluma* sp.	Ag–Fe	22	28	72	84	Present work
2	*Azadirachta indica*	Ag–Fe	20	30	70	85	[24]
3	*Moringa oleifera*	Ag–Fe	23	32	74	88	[25]
4	*Camellia sinensis*	Ag–Cu	21	31	71	86	[26]
5	*Aloe vera*	Ag–Ni	19	29	69	83	[27]
6	*Ocimum sanctum*	Fe–Cu	24	35	73	89	[28]
7	*Psidium guajava*	Ag–Fe	22	33	72	87	[29]
8	*Mangifera indica*	Ag–Cu	21	30	70	85	[30]
9	*Citrus limon*	Ag–Fe	23	34	74	88	[31]
10	*Punica granatum*	Ag–Cu	20	31	71	86	[32]
11	*Eucalyptus globulus*	Ag–Fe	22	32	73	87	[33]
12	*Calotropis procera*	Fe–Cu	24	36	75	90	[34]
13	*Phyllanthus emblica*	Ag–Ni	21	30	72	85	[35]
14	*Terminalia chebula*	Ag–Fe	23	34	74	88	[36]
15	*Curcuma longa*	Ag–Cu	22	33	73	87	[37]

INTERNATIONAL JOURNAL OF PHARMACY WITH MEDICAL SCIENCES
Peer Reviewed, Referred & Indexed Journal
E-ISSN:3068-2738
Vol.6, No. 2(2026)
www.ijpams.com

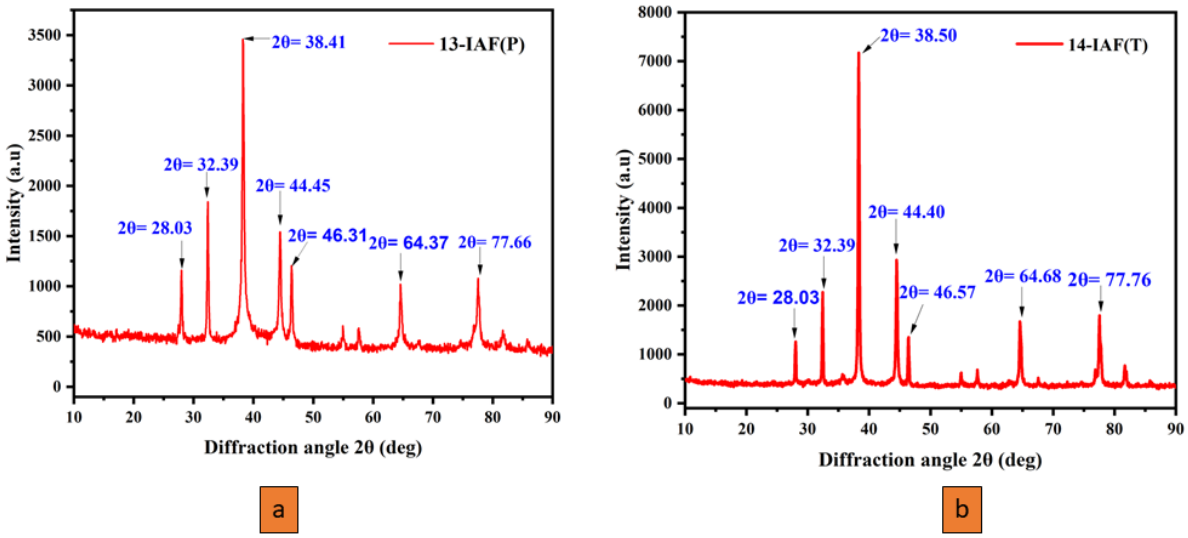

Figure 3 XRD analysis of a) Pre-extracted b) thermal treated green 'Ag–Fe' bimetallic nanoparticle

4.3 UV analysis

"UV-visible spectroscopy was used to examine the optical characteristics of the 'Ag–Fe' "bimetallic nanoparticles" produced by using Caralluma. Figures 4a and 4b display the absorption spectra of the IAF-P and "IAF-T" samples, respectively. The creation of nanoscale metal particles is indicated by the absorbance, which is significant in the ultraviolet region of both spectra and gradually decreases as it moves to the visible and near-infrared regions."'In case of the IAF-P sample there is the broad absorption feature at the 300-350 nm region which can be explained by a usual optical reaction related with the fact that 'Ag–Fe' 'nanoparticles' have been formed. This absorption band is broad which indicates that there may be polydisperse nanoparticles, and surface interactions with the phytochemical molecules of the *Caralluma* extract." The wide bands seen in green manufactured 'nanoparticles' are often attributed to the surface plasmon resonance (SPR) activity of Ag nanoparticles, as well as the charge-transfer transitions of iron oxide components. The slow decline in absorbance of the visible to the near-infrared area represents otherwise the existence of the nanoscale metallic structures with medium aggregation of the particles. "The absorption spectrum of the "IAF-T" sample has a comparable absorption pattern but the spectrum has a narrower and more pronounced absorption pattern at the same UV region (~320-340nm)." This enhancement of spectral definition is an indication of better nanoparticle formation and also better order in the structure after thermal treatment. The overall effect of the thermal processing is that it eliminates any organic compounds left behind by the plant extract thus allowing a better dispersion of the nanoparticle as well as enhancing electronic interactions between the two metals in the bimetallic system. "In comparison, the "IAF-T" sample has a relatively lower value of the overall absorbance intensity than IAF-P that can be explained by the fact that organic capping agents have become less abundant and the crystallinity of 'nanoparticles' has increased as a result of heating. The less rugged spectral profile of "IAF-T" is also an indication of less light scattering caused by partial elimination of plant biomolecules."

The optical characteristics of the two samples agree with the previous Ag-based and Fe-based 'nanoparticles' systems that have been reported to be plant mediated[38]. "Several investigations have indicated that, depending on the size, shape, and interaction with plant biomolecules, the absorption bands of the green synthesised Ag 'nanoparticles' are often seen at 300–450 nm [39]." Similarly, due of the ligand-to-metal charge transfer transitions, iron oxide 'nanoparticles' typically show high levels

of absorption in the UV area.“The synthesis of ‘Ag–Fe’ “bimetallic nanoparticles” stabilised by the phytochemical agent of “Caralluma extract” is therefore confirmed by these optical features combined in the current spectrum.”The formation of ‘nanoparticles’ is generally successful, according to the UV-visible analysis, and the comparative spectral characteristics demonstrate that thermal treatment improves the stability and organization of the nanoparticle structure, which may be advantageous for the ‘Ag–Fe’ nanomaterial system's optical and dielectric performance.

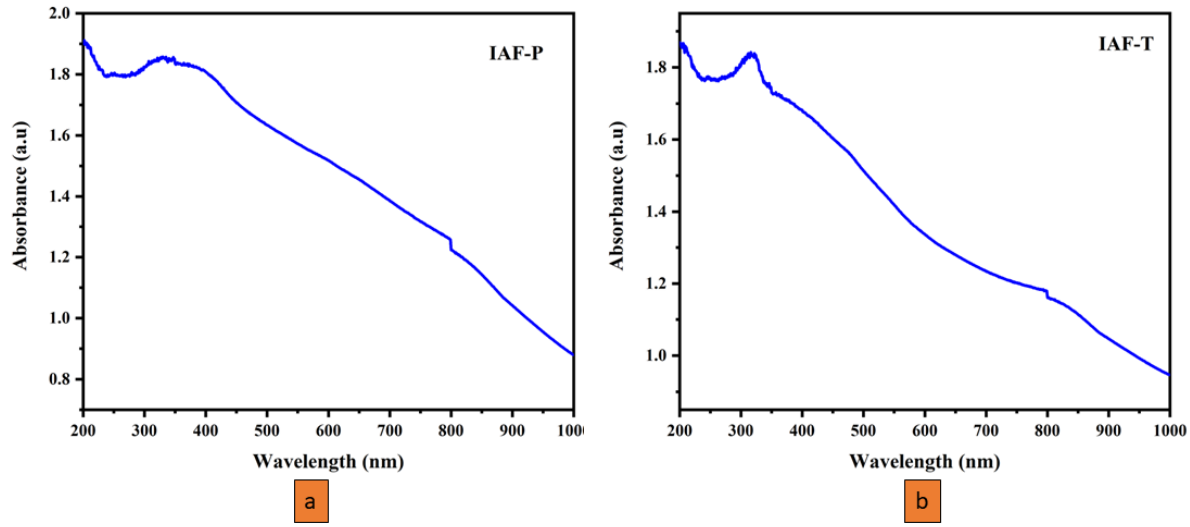

Figure 4 UV analysis of a) Pre-extracted b) thermal treated green ‘Ag–Fe’ bimetallic nanoparticle

4.4 SEM analysis

The raw “IAF-P” sample (Fig.5) exhibits a heterogeneous porous structure with substantial surface imperfections, as seen by scanning electron microscopy (SEM) micrographs. The nucleation and development of the ‘nanoparticles’ are aided by the presence of phytochemical substances in the Caralluma extract, as shown by the porous granular domains, which are composed of densely packed nanoscale particles, when the magnifications are raised (100 kX). “The micrographs captured at 50 kX and 25 kX also indicate that there are rough and porous surface areas with a lot of cavity structure implying that the raw material may contain organic residues and also lack complete coalescence of particles.” Smaller magnifications (10-25 kX) have sponge-like and honeycomb-type porous structures the porous interconnected pores and cavities are uniformly distributed throughout the matrix.” This kind of morphology suggests that there are loosely packed nanoparticle networks with large spaces. Moreover, some agglomerated formations are in the form of clustered and flake-like structures, which are frequent in the synthesis of ‘nanoparticles’ with the assistance of biomolecules because of intermolecular interactions of both biomolecules and metallic nuclei. Other comparable porous and agglomerated morphologies have been reported of green-synthesized Ag ‘nanoparticles’ prepared with *Azadirachta indica* and *Moringa oleifera* extracts in which organic capping molecules yielded sponge-like aggregated nano-particle features with unevenly distributed pores[40][41], [42].Thus, the SEM images ensure that the raw sample has very porous, agglomerated, and irregular surface morphology and that is the characteristic of bio-mediated ‘nanoparticles’ formation.

INTERNATIONAL JOURNAL OF PHARMACY WITH MEDICAL SCIENCES
Peer Reviewed, Referred & Indexed Journal
E-ISSN:3068-2738
Vol.6, No. 2(2026)
www.ijpams.com

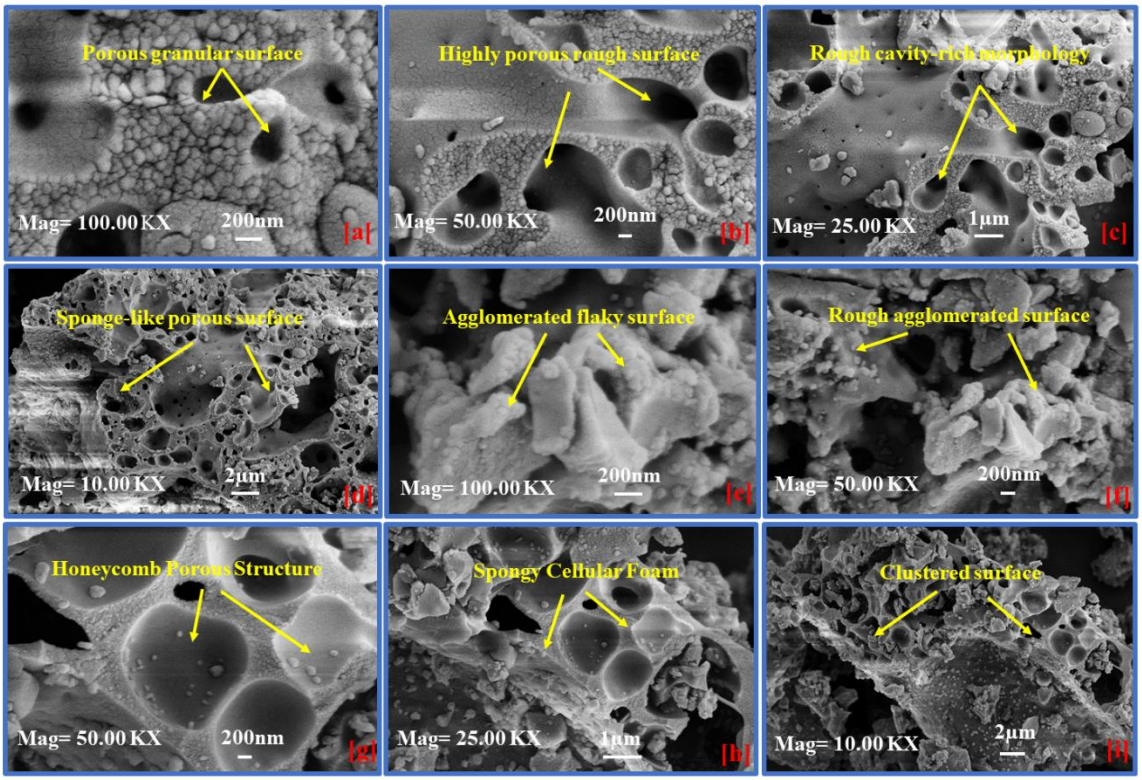

Figure 5 SEM analysis of pre-extracted green 'Ag–Fe' bimetallic nanoparticle

The SEM micrographs of the "IAF-T" sample thermally treated (Fig.6) show that there is an observable morphological change in the sample relative to the raw material. The high magnification (100 kX) reveals clear cylindric and rod-like granular structures on the surface, which means that the growth of the particles and the rearrangement of the structure are better during thermal processing. The 50 kX and 25 kX recorded images indicate porous rough surfaces with the formation of cavity and long cluster of particles, indicating that the heat treatment facilitates the diffusion of particles and part-sintering of the nanoparticles. At the middle and low magnifications (10-50 kX), the micrographs show surface agglomeration with rough porous domains and irregular shapes of particle cluster. Existence of granular porous surfaces and rod-like particle assemblies indicate that thermal treatment would help in the nurturing of crystallite growth and the structural stability of the bi-metallic nanoparticle system. In, "Ag–Fe" 'nanoparticles' produced with the help of *Citrus limon* and *Eucalyptus globulus* extracts have porous agglomerated structures in their raw form, which becomes compact and elongated particle networks after annealing because of the loss of organic capping agents and the improved diffusion of atoms[43], [44]. In general, the results of the SEM observations reveal that the raw sample (IAF-P) contains more sponge-like porous and highly agglomerated clusters of 'nanoparticles' formed as a result of biomolecule-mediated nucleation whereas the thermally treated sample "(IAF-T)" has a larger proportion of relatively compact granular and rod-like structures with less organic residues. The fact that thermal treatment improves structural arrangement and particle development in the plant-mediated system of Ag Fe bimetallic nanoparticle has been confirmed by the morphological development of porous aggregated networks to more defined particle assemblies.

INTERNATIONAL JOURNAL OF PHARMACY WITH MEDICAL SCIENCES
Peer Reviewed, Referred & Indexed Journal
E-ISSN:3068-2738
Vol.6, No. 2(2026)
www.ijpams.com

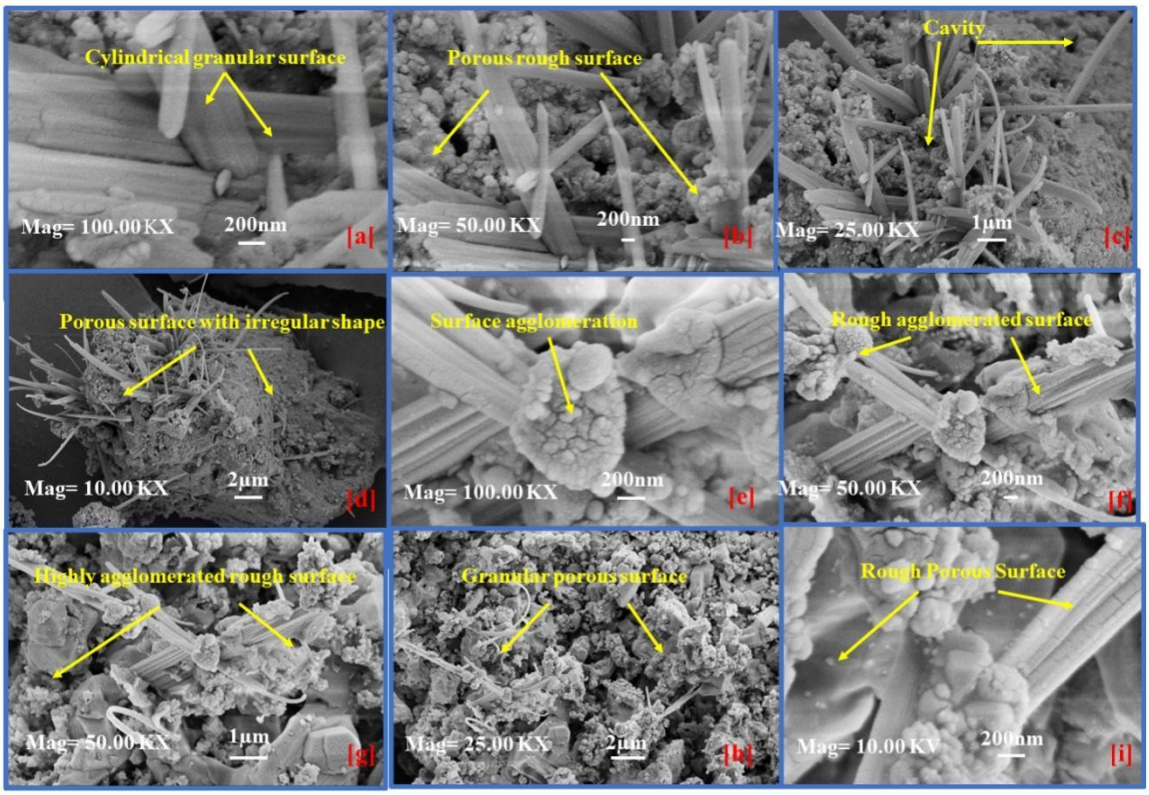

Figure 6 SEM analysis of thermal treated green 'Ag–Fe' bimetallic nanoparticle

4.5 Dielectric property analysis

Dielectric behavior of the plant-mediated "IAF-P" sample was studied as a frequency dependent behavior ranging between about "10 -10^3 Hz."As the frequency increases, the real part of the dielectric constant (ε) rises sharply at low frequencies before gradually falling off.The Maxwell-Wagner interfacial polarisation mechanism, in combination with the Koop theory, may be used to explain the frequency-dependent behaviour of heterogeneous nanostructured materials. In this theory, the material is modelled as a system of conducting grains in poor conductor grain borders. Additionally, at lower frequencies, charge carriers will be concentrated in the grain boundaries and interfaces, resulting in a high degree of space-charge polarisation and an increase in dielectric constant values. As the frequency of the alternating electric field increases, the dipoles and charge carriers are unable to keep the material polarised, which results in a decreasing epsilon. Additionally, the dielectric loss or imaginary fraction of the dielectric constant (ε') diminishes with increasing frequency. The significant dielectric loss in the low frequency range is caused by the motion of charge carriers and the polarisation processes at the interface. The modulus representation also aids in this behaviour since the real and imaginary components of the electric modulus are very small at low frequencies and gradually increase at high frequencies.This is evidence of electrode polarization inhibition and conversion of long-range charge carrier movement to localized relaxation. The conduction mechanism is regulated by the hopping of charge carriers between localised states, as seen by the gradual rise in AC conductivity (σ) of the "IAF-P" sample with frequency. Plant extracts may contain phytochemical residues that affect the raw sample's dielectric response through mechanisms like charge trapping and interfacial polarisation.

INTERNATIONAL JOURNAL OF PHARMACY WITH MEDICAL SCIENCES
Peer Reviewed, Referred & Indexed Journal
E-ISSN:3068-2738
Vol.6, No. 2(2026)
www.ijpams.com

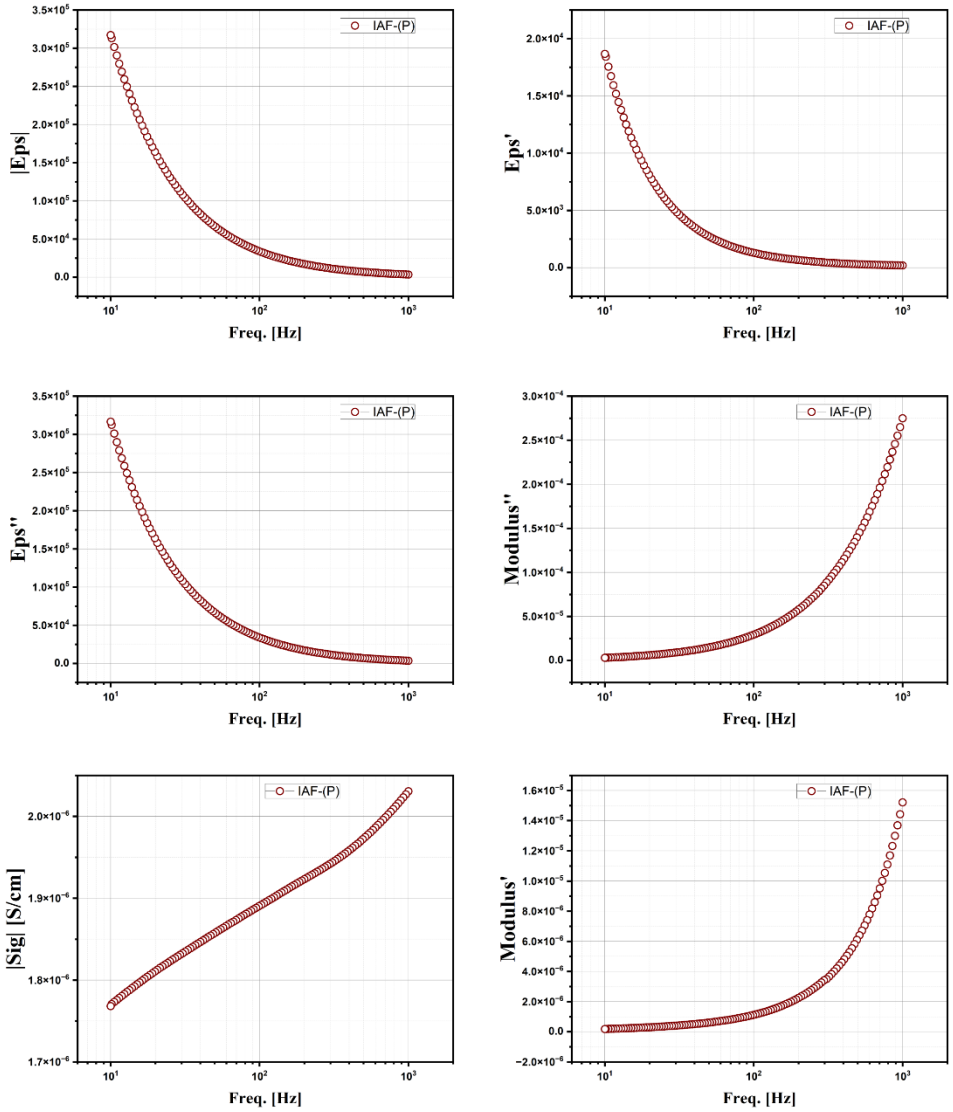

Figure 7 Dielectric properties analysis of Pre-extracted green 'Ag–Fe' bimetallic nanoparticle

The frequency-dependent dielectric behaviour of the thermally treated IAF-T sample is not much different than IAF-P. The dielectric constant (ε) is steadily reduced by increasing frequency but once more is explained by the fact that space-charge polarization is reduced at higher frequencies. Nonetheless, the values of the dielectric constant of "IAF-T" sample are relatively small in comparison to the raw sample over the whole range of frequencies. This decrease is explained by the thermal elimination of phytochemical capping reagents and increased crystallinity of the 'nanoparticles' which decreases the interfacial polarization contribution. The dielectric loss (ε) also falls as the frequency increases meaning that, the energy dissipation in the material is more at low frequencies and minimum at higher frequencies. The thermal treated sample has relatively lower values of dielectric loss, relative to the raw one, implying that the sample has a better structural ordering and lesser defect density following the heat treatment. The electric modulus plots indicate that the electric modulus is continuously increasing with the frequency, which proves the presence of the dielectric relaxation processes in the nanoparticle system. Furthermore, the "IAF-T" sample exhibits a greater frequency-dependent AC conductivity, which was a consequence of the thermal treatment's reduction of the grain

boundary resistance and the improved charge transportation resulting from the crystal ordering. Frequency dependent polarization behaviour characteristic of nanostructured materials is clearly evident in the dielectric response of the two samples. In comparison, the raw sample (IAF-P) has a greater dielectric constant and dielectric loss due to the organic compounds removed from the plants, which create polarisation of the interface and charge trapping. Conversely, thermal processed sample (IAF-T) has lower dielectric constant and dielectric loss and slightly increased electrical conductivity which may be explained by better crystallinity and lower organic content of samples following the thermal treatment. This data implies that thermal treatment improves structural order and allows a more efficient movement of charge in the 'Ag–Fe' nanoparticle system thus increasing the dielectric stability of the material.

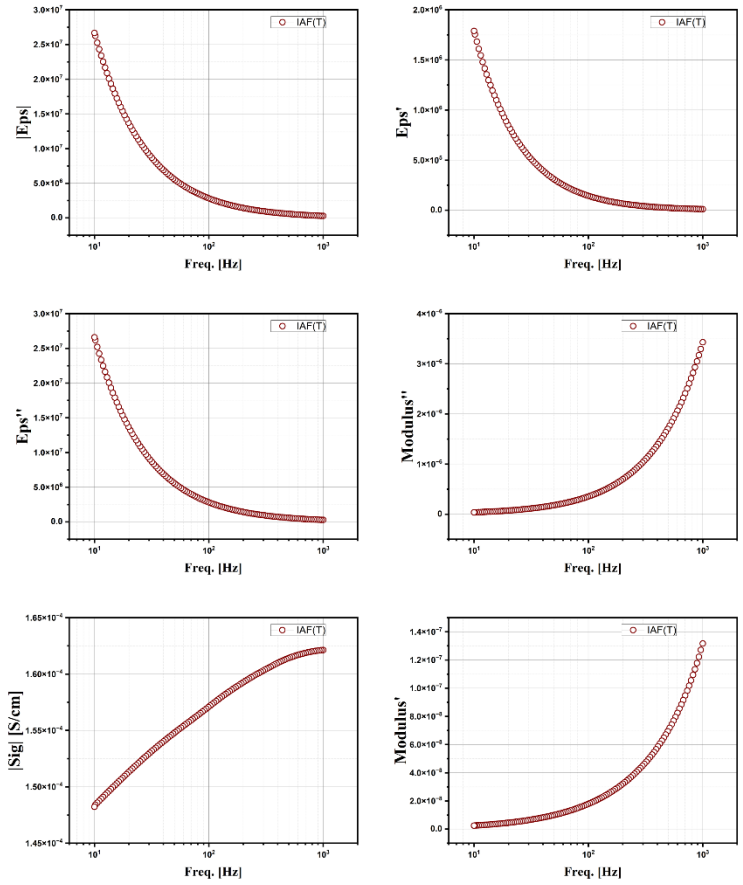

Figure 8 Dielectric properties analysis of thermal treated green 'Ag–Fe' bimetallic nanoparticle

4.6 Binding to target evaluation

The docking study has successfully identified from plant derivatives that interact favorably with specific protein target (3K35). Luteolin-4'-O-neohesperidoside from *Caralluma Umbellata* stand out as the most promising compounds due to their strong interaction energies and favorable docking scores. "This compound may have potential therapeutic applications, particularly in systems where their binding stability and interaction strength. Luteolin-4'-O-neohesperidoside (from Caralluma Umbellata) shows a C-Docker energy of 82.8541, indicating a favorable docking pose. Despite this, its C-Docker Interaction energy of -40.0722 is moderate compared to other compounds, suggesting that while the compound fits well into the receptor, its binding strength might not be as high as other ligands."

INTERNATIONAL JOURNAL OF PHARMACY WITH MEDICAL SCIENCES
Peer Reviewed, Referred & Indexed Journal
E-ISSN:3068-2738
Vol.6, No. 2(2026)
www.ijpams.com

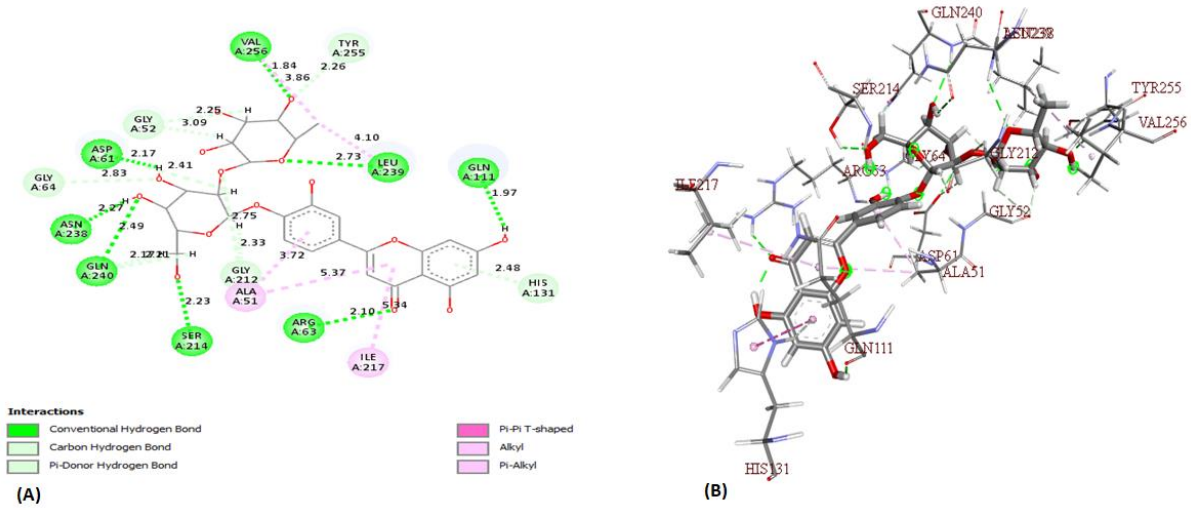

Figure 9: 2D and 3D interaction of Luteolin-4'-O-neohesperidoside to target protein for antidiabetic efficacy

The molecule Luteolin-4'-O-neohesperidoside is a flavonoid glycoside, meaning it consists of a flavonoid structure (luteolin) bound to a sugar (neohesperidoside) through a covalent glycosidic bond. This bond forms between the hydroxyl group of luteolin and the sugar molecule, making the compound water-soluble and more bioavailable. "Flavonoids like luteolin have hydroxyl (-OH) groups, which can form hydrogen bonds with other hydroxyl groups or with polar residues in proteins or enzymes." The sugar moiety can also form hydrogen bonds with water molecules or with amino acid side chains in protein-ligand interactions. The aromatic rings of luteolin may participate in π-π stacking interactions with aromatic amino acids (such as phenylalanine, tyrosine, or tryptophan) in the binding site of a protein or receptor. The hydrophobic regions of luteolin's aromatic structure can engage in van der Waals interactions with hydrophobic patches in receptor or enzyme binding sites. The binding and interaction of Luteolin-4'-O-neohesperidoside with 3K35 can be seen in Figure 9.

4.7 DPPH Radical Scavenging Assay (Antioxidant activity)

Caralluma Umbellata extract demonstrated a strong antioxidant activity in the DPPH Radical Scavenging Assay, which measured its capacity to neutralise the DPPH free radical. The plant extract is added to a solution of DPPH, a stable nitrogen-centered radical with a deep violet hue, in order for the assay to function. When the DPPH radical is exposed to an antioxidant, like the one in Sample 13, it is decreased and turns pale yellow instead of violet. This transformation happens as a result of the antioxidant neutralising the radical by giving it an electron or a hydrogen atom. "Three different doses of Caralluma Umbellata extract were tested: 20 µg/mL, 40 µg/mL, and 60 µg/mL. The inhibition percentages for Sample 13 were determined by comparing the sample to the control (DPPH without antioxidant) at an absorbance of 0.81 and then calculating the decrease in absorbance at 517 nm. At 20 µg/mL, Sample 13 achieved a % inhibition of 26±2.9%, indicating a mild antioxidant activity. The activity improved as the concentration increased. At 40 µg/mL, the % inhibition rose to 32±1.9%, and at 60 µg/mL, it reached 46±2.7%." This progressive increase in % inhibition shows that the extract from Sample 13 exhibits a dose-dependent antioxidant activity, meaning that higher concentrations of the extract are more effective at scavenging free radicals. The results from *Caralluma Umbellata* extract demonstrate a moderate antioxidant potential, particularly at the higher concentration, where it was able to neutralize almost half of the DPPH radicals. These findings suggest that the plant extract in Sample 13 contains compounds, possibly phenolics or flavonoids that have the ability to scavenge free radicals

effectively. Consequently, Sample 13 could be considered a promising natural antioxidant candidate for further exploration in pharmaceutical or nutraceutical applications.

4.8 Anti-fungal activity of plant extract

Caralluma Umbellata extract was tested using the agar well diffusion method against three fungal strains in the antifungal activity assay: Aspergillus fumigatus (Figure 10 A), Candida tropicalis (Figure 10 B), and Trichophyton rubrum (Figure 10 C). "The size of the clear "zone of inhibition (ZOI)" that forms around the well indicates how well the test ingredient "(Caralluma Umbellata extract)" diffuses through the agar medium and inhibits fungal growth. *Caralluma Umbellata* extract was tested at a concentration of 50–100 µL in the wells of the agar plates inoculated with fungal cultures."The zone of inhibition (ZOI) was measured in millimetres during a 24- to 48-hour incubation period at the proper temperature. According to the findings, the extract from Caralluma umbellata showed considerable antifungal efficacy against each of the three tested fungal strains. "Trichophyton rubrum had a zone of inhibition of 4.3±0.04 mm, Candida tropicalis had a somewhat smaller zone of 3.5±0.5 mm, and Aspergillus fumigatus had a zone of inhibition of 4.5±0.5 mm, indicating modest inhibition."

These results suggest that *Caralluma Umbellata* extract has a moderate ability to inhibit fungal growth, although its activity is weaker compared to samples showing larger inhibition zones (typically above 5 mm). Candida tropicalis, in particular, showed the smallest sensitivity to *Caralluma Umbellata* extract, with a smaller inhibition zone compared to the other strains. This could imply that the antifungal compounds present in *Caralluma Umbellata* extract are more effective against certain fungal species than others. The bioactive substances in the Caralluma Umbellata extract may interact with the fungal cell wall or interfere with vital cellular functions, which could explain the reported antifungal effects.However, given the moderate size of the inhibition zones, further studies including dose-response evaluations, "Minimum Inhibitory Concentration (MIC)" testing, and formulation development are necessary to better understand the potential of *Caralluma Umbellata* extract as an antifungal agent.

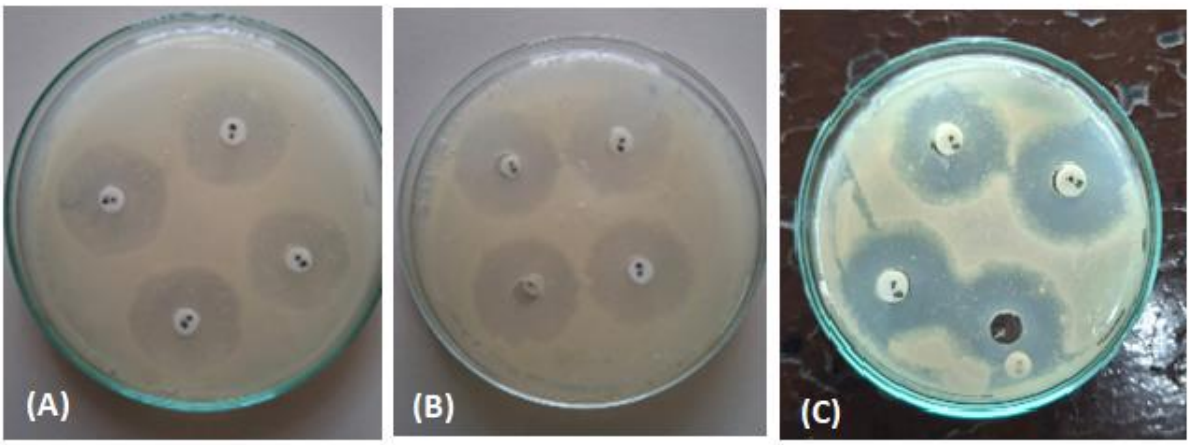

Figure 10: Zone of inhibition in mm observed for selected plant extract on three different fungal species.

4.9 Anti diabetic assessment by α-Amylase Inhibition Assay

Caralluma Umbellata extract in the α-Amylase Inhibition Assay exhibited varying degrees of enzyme inhibition at different concentrations, showcasing its potential as an antidiabetic agent. "At a concentration of 50 µg/mL, the absorbance value was recorded at 0.662, corresponding to a 23% inhibition of α-amylase activity. This indicates mild inhibition at this concentration. Upon increasing the concentration to 100 µg/mL, the absorbance decreased to 0.370, and the inhibition rose significantly to 57%, indicating a stronger inhibitory effect. At the highest concentration tested (200 µg/mL), the

absorbance value further decreased to 0.344, and the inhibition reached 60%. This marked increase in inhibition at higher concentrations suggests that *Caralluma Umbellata* extract has a dose-dependent effect on α-amylase activity. The inhibition observed at different concentrations can be attributed to the competitive or non-competitive interactions between the phytochemicals present in *Caralluma Umbellata* extract and the α-amylase enzyme. As the concentration of the plant extract increases, the bioactive compounds such as flavonoids, phenolic compounds, tannins, alkaloids, and saponins—likely interact more effectively with the enzyme, reducing its activity and hindering starch hydrolysis. This leads to a decrease in the formation of reducing sugars, as indicated by the lower absorbance values measured at 540 nm after the reaction." The results suggest that *Caralluma Umbellata* extract has moderate to strong α-amylase inhibitory activity, especially at higher concentrations, which could potentially help in controlling postprandial blood sugar levels in diabetic individuals. These findings position *Caralluma Umbellata* extract as a promising candidate for further pharmacological investigation and in vivo testing to explore its therapeutic potential.

5. Conclusion

The Green synthesis approach, which is ecologically benign, was used to produce 'Ag–Fe' "bimetallic nanoparticles" utilising Caralluma plant extract. The presence of phytochemical functional groups that stabilised and reduced metal ions throughout the nanoparticle formation process was verified by FTIR analysis."After heating, the sample's crystallinity index rose from 72% to 84%, suggesting a higher structural order; XRD analysis revealed that the nanoparticles' crystal size had changed from 22 nm to 28 nm.UV-vis spectroscopy revealed a distinctive absorption band between 300 and 350 nm, indicating the optical response of the 'Ag–Fe' nanoparticle system." The micrographs of the SEM showed that the raw 'nanoparticles' had highly porous and agglomerated forms and the thermal treatment was characterized by relatively compact granular and rod-like forms through growth of the particles and removal of organic residues partially. Dielectric experiments demonstrated that the dielectric constant and dielectric loss reduced with increasing frequency, as expected by the Maxwell-Wagner interfacial polarisation process."The thermally treated 'nanoparticles' had a lower dielectric loss and a little bit higher AC conductivity, which means that the charge transport was enhanced with the increase of crystallinity."Overall, the results confirm that synthesising 'Ag–Fe' "bimetallic nanoparticles" using Caralluma is a practical way to create'nanoparticles' that are structurally stable and have great potential as electronic, catalytic, and functional nanomaterials.

Acknowledgement

We expresses sincere gratitude to the supporting institutions and laboratories that facilitated this research work.

Conflict of Interest

We declare no conflict of interest.

Author Contributions

K Sirisha Rani conducted the experiments, data analysis, and manuscript preparation. Academic supervision was provided by the research guide.

Data Availability

The corresponding author may be contacted with any legitimate request to get the data supporting this study's findings.

References

[1] S. Iravani, "Green synthesis of metal 'nanoparticles' using plants," *Green Chem.*, vol. 13, no. 10, pp. 2638–2650, 2011, doi: 10.1039/C1GC15386B.

[2] S. Ahmed, M. Ahmad, B. L. Swami, and S. Ikram, "A review on plants extract mediated synthesis of silver 'nanoparticles' for antimicrobial applications: A green expertise," *J. Adv. Res.*, vol. 7, no. 1, pp. 17–28, 2016, doi: https://doi.org/10.1016/j.jare.2015.02.007.

[3] A. K. Mittal, Y. Chisti, and U. C. Banerjee, "Synthesis of metallic 'nanoparticles' using plant extracts," *Biotechnol. Adv.*, vol. 31, no. 2, pp. 346–356, 2013, doi: https://doi.org/10.1016/j.biotechadv.2013.01.003.

[4] V. K. Sharma, R. A. Yngard, and Y. Lin, "Silver nanoparticles: Green synthesis and their antimicrobial activities," *Adv. Colloid Interface Sci.*, vol. 145, no. 1, pp. 83–96, 2009, doi: https://doi.org/10.1016/j.cis.2008.09.002.

[5] P. Mohanpuria, N. K. Rana, and S. K. Yadav, "Biosynthesis of nanoparticles: technological concepts and future applications," *J. Nanoparticle Res.*, vol. 10, no. 3, pp. 507–517, 2008, doi: 10.1007/s11051-007-9275-x.

[6] P. Singh, Y.-J. Kim, D. Zhang, and D.-C. Yang, "Biological Synthesis of 'nanoparticles' from Plants and Microorganisms," *Trends Biotechnol.*, vol. 34, no. 7, pp. 588–599, Jul. 2016, doi: 10.1016/j.tibtech.2016.02.006.

[7] M.-C. Daniel and D. Astruc, "Gold Nanoparticles: Assembly, Supramolecular Chemistry, Quantum-Size-Related Properties, and Applications toward Biology, Catalysis, and Nanotechnology," *Chem. Rev.*, vol. 104, no. 1, pp. 293–346, Jan. 2004, doi: 10.1021/cr030698+.

[8] M. Brust, M. Walker, D. Bethell, D. J. Schiffrin, and R. Whyman, "Synthesis of thiol-derivatised gold 'nanoparticles' in a two-phase Liquid–Liquid system," *J. Chem. Soc. Chem. Commun.*, no. 7, pp. 801–802, 1994, doi: 10.1039/C39940000801.

[9] S. Sun, C. B. Murray, D. Weller, L. Folks, and A. Moser, "Monodisperse FePt 'nanoparticles' and Ferromagnetic FePt Nanocrystal Superlattices," *Science (80-.).*, vol. 287, no. 5460, pp. 1989–1992, Mar. 2000, doi: 10.1126/science.287.5460.1989.

[10] H. Jiang, X. Pan, C. Liu, R. Ma, and Y. Tian, "Recent advances in utilization of tamarind seed as a sustainable source for development of food packaging," *Trends Food Sci. Technol.*, p. 105534, 2026, doi: https://doi.org/10.1016/j.tifs.2026.105534.

[11] K. Subramani, P. Wutthithien, R. Saha, P. Lindblad, and A. Incharoensakdi, "Characterization and potentiality of plant-derived silver 'nanoparticles' for enhancement of biomass and hydrogen production in Chlorella sp. under nitrogen deprived condition," *Chemosphere*, vol. 361, p. 142514, 2024, doi: https://doi.org/10.1016/j.chemosphere.2024.142514.

[12] M. Sahu *et al.*, "Synthesis and characterization of ethanolic extract of nutgalls of the plant Quercus infectoria silver nitrate 'nanoparticles' incorporated chitosan based scaffold, and their in-silico study for wound healing activity," *Results in Surfaces and Interfaces*, vol. 18, p. 100379, 2025, doi: https://doi.org/10.1016/j.rsurfi.2024.100379.

[13] Z. Zulfiqar *et al.*, "Plant-mediated green synthesis of silver nanoparticles: Synthesis, characterization, biological applications, and toxicological considerations: A review," *Biocatal. Agric. Biotechnol.*, vol. 57, p. 103121, 2024, doi: https://doi.org/10.1016/j.bcab.2024.103121.

[14] A. Noori *et al.*, "Silver 'nanoparticles' in plant health: Physiological response to phytotoxicity and oxidative stress," *Plant Physiol. Biochem.*, vol. 209, p. 108538, 2024, doi: https://doi.org/10.1016/j.plaphy.2024.108538.

[15] I. O. Amao, A. O. Okesola, T. O. Ajiboye, V. O. Animasahun, and H. O. Dada-Adegbola, "Antimicrobial Potency of the Biosynthesized Silver 'nanoparticles' (AgNPs) on Methicillin-Resistant Staphylococcus aureus (MRSA) Using Bridelia ferruginea Benth Plant Extract," *Curr. Nanomater.*, vol. 10, no. 2, pp. 198–208, 2025, doi: https://doi.org/10.2174/0124054615292315240318062929.

[16] R. Kumar Singh, D. Nallaswamy, S. Rajeshkumar, and S. S. Varghese, "Green synthesis of silver 'nanoparticles' using neem and turmeric extract and its antimicrobial activity of plant mediated silver nanoparticles," *J. Oral Biol. Craniofacial Res.*, vol. 15, no. 2, pp. 395–401,

2025, doi: https://doi.org/10.1016/j.jobcr.2025.02.005.

[17] M. A. Khan, A. Masood, K. Ali, N. Farid, A. Bashir, and M. S. Dar, "Green synthesis of silver, starch, and zinc oxide mediated 'nanoparticles' with probiotics and plant extracts, their characterization and anti-bacterial activity," *Microb. Pathog.*, vol. 196, p. 107012, 2024, doi: https://doi.org/10.1016/j.micpath.2024.107012.

[18] M. A. Shereen *et al.*, "Plant extract preparation and green synthesis of silver 'nanoparticles' using Swertia chirata: Characterization and antimicrobial activity against selected human pathogens," *Heliyon*, vol. 10, no. 6, p. e28038, 2024, doi: https://doi.org/10.1016/j.heliyon.2024.e28038.

[19] D. O. D. Leite *et al.*, "Influence of methanolic extracts from seeds and pulp of Annona squamosa L. on osmotic and morphological fragility in human erythrocytes," *Curr. Res. Toxicol.*, vol. 4, p. 100103, 2023, doi: https://doi.org/10.1016/j.crtox.2023.100103.

[20] A. Ripanda *et al.*, "Removal of lamivudine from synthetic solution using jamun seed (Syzygium cumini) biochar adsorbent," *Emerg. Contam.*, vol. 9, no. 3, p. 100232, 2023, doi: https://doi.org/10.1016/j.emcon.2023.100232.

[21] A. Y. Moussa, S. A. Siddiqui, E. A. Elhawary, K. Guo, S. Anwar, and B. Xu, "Phytochemical constituents, bioactivities, and applications of custard apple (Annona squamosa L.): A narrative review," *Food Chem.*, vol. 459, p. 140363, 2024, doi: https://doi.org/10.1016/j.foodchem.2024.140363.

[22] R. Rajan, K. Chandran, S. L. Harper, S.-I. Yun, and P. T. Kalaichelvan, "Plant extract synthesized silver nanoparticles: An ongoing source of novel biocompatible materials," *Ind. Crops Prod.*, vol. 70, pp. 356–373, 2015, doi: https://doi.org/10.1016/j.indcrop.2015.03.015.

[23] M. I. Ali, M. E. Omar, and A. A. Al-Abbasi, "Removal of silver 'nanoparticles' from aqueous solution using cellulose extracted from Traganum Nudatum plant activated by zinc chloride," *Next Nanotechnol.*, vol. 7, p. 100190, 2025, doi: https://doi.org/10.1016/j.nxnano.2025.100190.

[24] F. Bahador, R. Foroutan, H. Esmaeili, and B. Ramavandi, "Enhancement of the chromium removal behavior of Moringa oleifera activated carbon by chitosan and iron oxide 'nanoparticles' from water," *Carbohydr. Polym.*, vol. 251, p. 117085, 2021, doi: https://doi.org/10.1016/j.carbpol.2020.117085.

[25] F. Ogundolie, G. Adebayo-gege, R. A. Aliyu, Q. Ozegbe, A. J. Muhammed, and T. D. Alabi, "Green Silver 'nanoparticles' Synthesized from Moringa Oleifera Stem Bark Elicits Effective Antidiabetic Effect in Alloxan-Induced (Type I) Diabetic Wistar Rats," *J. Pharmacol. Exp. Ther.*, vol. 389, p. 81, 2024, doi: https://doi.org/10.1124/jpet.081.926380.

[26] N. Lehman, R. Phengthai, and W. Chinpa, "Effect of Moringa oleifera Pod Husk Fibers on the Properties of Gelatin-Based Biocomposite," *J. Polym. Environ.*, vol. 26, no. 4, pp. 1405–1414, 2018, doi: 10.1007/s10924-017-1042-1.

[27] N. L. Mojela, K. Pillay, and P. P. Komane, "Synthesis and application of silver 'nanoparticles' from lemon peel extract and other local plant extracts for detection of 'blood' at crime scene," *Forensic Sci. Int.*, vol. 365, p. 112257, 2024, doi: https://doi.org/10.1016/j.forsciint.2024.112257.

[28] S. Shahzadi, S. Fatima, Q. ul ain, Z. Shafiq, and M. R. S. A. Janjua, "A review on green synthesis of silver 'nanoparticles' (SNPs) using plant extracts: a multifaceted approach in photocatalysis, environmental remediation, and biomedicine," *RSC Adv.*, vol. 15, no. 5, pp. 3858–3903, 2025, doi: https://doi.org/10.1039/d4ra07519f.

[29] G. Kah, O. A. Adelusi, S. Gbashi, P. M. Awafong, and P. B. Njobeh, "Antifungal and antimycotoxin activity of plant-synthesized silver 'nanoparticles' (AgNPs): A novel approach

to combat food contamination," *Food Microbiol.*, vol. 135, p. 104979, 2026, doi: https://doi.org/10.1016/j.fm.2025.104979.

[30] J. B. George, N. Cyril, J. P. Ramachandran, R. Radhamony, V. P. Sylas, and S. John, "Novel approach to gold ion detection in aqueous solutions using silver 'nanoparticles' synthesized from the seed extract of mangrove associate plant Thespesia populnea," *Results in Surfaces and Interfaces*, vol. 21, p. 100634, 2025, doi: https://doi.org/10.1016/j.rsurfi.2025.100634.

[31] N. H. Kurshed, A. A. Khadom, R. K. Ismail, S. K. Mohuee, N. K. Ahmed, and A. Alamiery, "Green biosynthesis of silver 'nanoparticles' from Citrus aurantium leaves plant as corrosion inhibitor for carbon steel in sulfuric acid," *Next Nanotechnol.*, vol. 9, p. 100331, 2026, doi: https://doi.org/10.1016/j.nxnano.2025.100331.

[32] W. Dagher, A. Alassod, M. F. Al Hinnawi, I. Alghoraibi, A. Taher, and M. Alnhlaoui, "Characterization and antibacterial effect of green-synthesised silver 'nanoparticles' using different extraction methods from Ziziphus spina-christi (Sidr) leaf extract collected from Syria," *RSC Adv.*, vol. 15, no. 42, pp. 35642–35659, 2025, doi: https://doi.org/10.1039/d5ra05214a.

[33] R. Santhosh and P. Sarkar, "Fabrication of jamun seed starch/tamarind kernel xyloglucan bio-nanocomposite films incorporated with chitosan 'nanoparticles' and their application on sapota (Manilkara zapota) fruits," *Int. J. Biol. Macromol.*, vol. 260, p. 129625, 2024, doi: https://doi.org/10.1016/j.ijbiomac.2024.129625.

[34] L. Madaniyah, S. Fiddaroini, E. K. Hayati, M. F. Rahman, and A. Sabarudin, "Biosynthesis, characterization, and in-vitro anticancer effect of plant-mediated silver 'nanoparticles' using Acalypha indica Linn: In-silico approach," *OpenNano*, vol. 21, p. 100220, 2025, doi: https://doi.org/10.1016/j.onano.2024.100220.

[35] K. Deka *et al.*, "Understanding the mechanism underlying the green synthesis of metallic 'nanoparticles' using plant extract(s) with special reference to Silver, Gold, Copper and Zinc oxide nanoparticles," *Hybrid Adv.*, vol. 9, p. 100399, 2025, doi: https://doi.org/10.1016/j.hybadv.2025.100399.

[36] C. Nirmala, H. K. Bajwa, and S. Oinam, "Bamboo mediated green synthesis of silver nanoparticles-A new approach towards utilization of an underutilized plant," *Adv. Bamboo Sci.*, vol. 6, p. 100061, 2024, doi: https://doi.org/10.1016/j.bamboo.2024.100061.

[37] N. Rana, P. Kumari, M. Bala, R. Kumar, and S. Kumar, "Eco-friendly synthesis and bioactivity of Acacia catechu heartwood -derived silver oxide nanoparticles," *Sustain. Chem. One World*, vol. 9, p. 100168, 2026, doi: https://doi.org/10.1016/j.scowo.2025.100168.

[38] Y. Jan *et al.*, "Characterization of jamun (Syzygium cumini) juice fortified with nanoemulsified vitamin D3: In vitro and in vivo assessment of its nutraceutical value and anti-diabetic potential," *Food Chem. X*, vol. 25, p. 102133, 2025, doi: https://doi.org/10.1016/j.fochx.2024.102133.

[39] S. Tripathi, S. Mahra, S. Sharma, S. Mathew, and S. Sharma, "Interaction of silver 'nanoparticles' with plants: A focus on the phytotoxicity, underlying mechanism, and alleviation strategies," *Plant Nano Biol.*, vol. 9, p. 100082, 2024, doi: https://doi.org/10.1016/j.plana.2024.100082.

[40] N. Madubuonu *et al.*, "Biosynthesis of iron oxide 'nanoparticles' via a composite of Psidium guavaja-Moringa oleifera and their antibacterial and photocatalytic study," *J. Photochem. Photobiol. B Biol.*, vol. 199, p. 111601, 2019, doi: https://doi.org/10.1016/j.jphotobiol.2019.111601.

[41] T. O. Siyanbola *et al.*, "Development of functional polyurethane-cenosphere hybrid composite coatings from ricinus communis seed oil," *Sci. African*, vol. 20, 2023, doi:

10.1016/j.sciaf.2023.e01711.

[42] S. Ramadevi *et al.*, "Effect of traditionally used herb Pedalium murex L. and its active compound pedalitin on urease expression – For the management of kidney stone," *Saudi J. Biol. Sci.*, vol. 27, no. 3, pp. 833–839, 2020, doi: 10.1016/j.sjbs.2020.01.014.

[43] N. A. Al-Tayyar, A. M. Youssef, and R. Al-hindi, "Antimicrobial food packaging based on sustainable Bio-based materials for reducing foodborne Pathogens: A review," *Food Chem.*, vol. 310, no. November 2019, p. 125915, 2020, doi: 10.1016/j.foodchem.2019.125915.

[44] R. B. Kalengyo, M. G. Ibrahim, M. Fujii, and M. Nasr, "Utilizing orange peel waste biomass in textile wastewater treatment and its recyclability for dual biogas and biochar production: a techno-economic sustainable approach," *Biomass Convers. Biorefinery*, vol. 14, no. 16, pp. 19875–19888, 2024, doi: 10.1007/s13399-023-04111-1.